Supporting information: Engineering a Functional small RNA Negative Autoregulation Network with Model-guided Design

Chelsea Y. Hu[1,4,#], Melissa K. Takahashi[1,2,#], Yan Zhang[1,3], Julius B. Lucks[4]*

1 – Robert F. Smith School of Chemical and Biomolecular Engineering, Cornell University, Ithaca NY
2 – Institute for Medical Engineering and Science, Massachusetts Institute of Technology, Cambridge, MA
3 – School of Chemical and Biomolecular Engineering, Georgia Institute of Technology, Atlanta, GA
4 -- School of Chemical and Biological Engineering, Northwestern University, Evanston, IL
- Co-first authorship

Table of contents

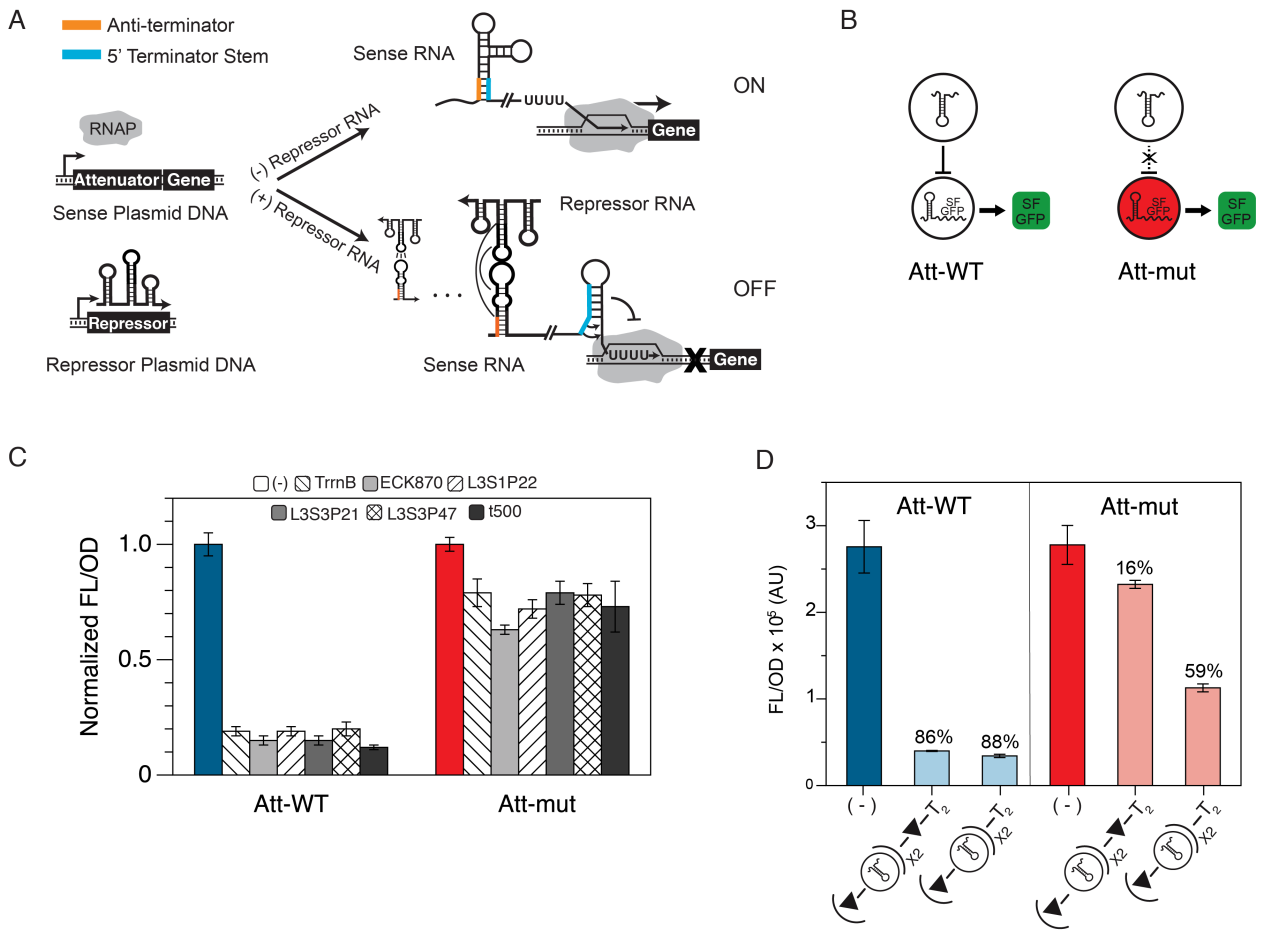

Figure S1. The effect of terminator identity on attenuator function. (A) Natural repressor-RNA transcriptional repression in the pT181 attenuator. Transcription of a downstream gene is undisrupted when the repressor RNA is absent. When the repressor RNA is present, it interacts with the attenuator RNA to form a transcriptional terminator hairpin. Therefore, the transcription of the downstream gene is turned off. (B) Schematics of basic sRNA repression constructs testing both cognate and non-cognate (orthogonal) regulation. (C) *In vivo* test of 5 new terminators compared against TrrnB in the context of the sRNA repressor. Error bars represent standard deviations over nine biological replicates. L3S3P21 was chosen for the rest of this work. (D) *In vivo* orthogonality test of double (tandem) repressors. Adding a ribozyme (triangle) between the terminator and repressor construct restores orthogonality. Error bars represent standard deviations over three biological replicates.

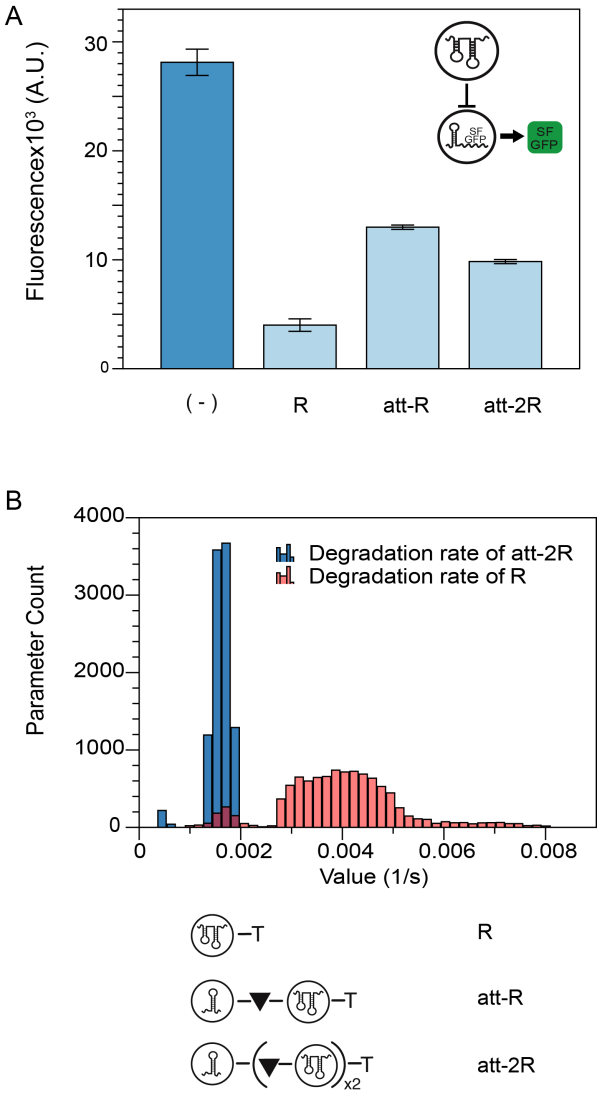

Figure S2. Re-plots of previous findings on pT181 sRNA repression strength and degradation rates. (A) Re-plot of *in vivo* attenuator repression characterization from Lucks et all 2011[1]. The repression efficiency of pT181 repressor antisense (R) is reduced when an attenuator sequence is placed upstream (att-R). Using two copies of repressors in tandem (att-2R) increases the repression strength slightly. (B) Re-plot of degradation parameter distributions for different repressor constructs determined from cell-free TX-TL experiments in Hu *et al.* 2015[2]. The degradation rate of the bare pT181 repressor sRNA (R, red) is faster than the degradation rate of the att-2R version (blue).

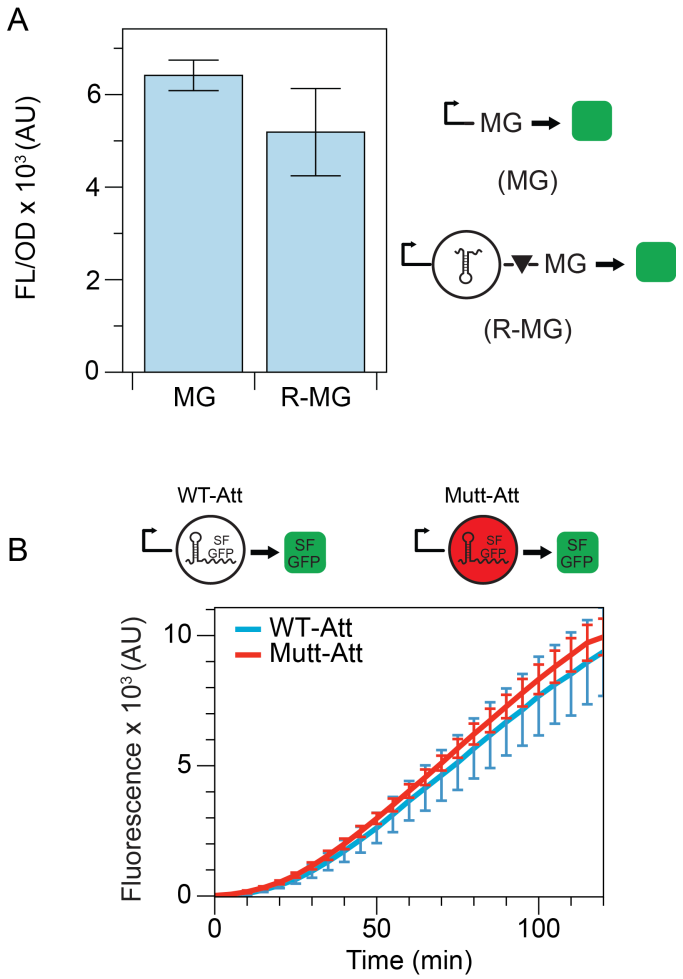

Figure S3. Characterization of malachite green and SFGFP expression constructs. (A) End point fluorescent measurement at the end of a 2-hour TX-TL reaction with a constitutive promoter driving malachite-green aptamer expression (MG) compared with a version containing a repressor-ribozyme sequence in between the promoter and the MG aptamer (R-MG). This result indicates some reduction in MG transcription caused by the presence of the repressor-ribozyme sequence. The ribozyme is indicated by a triangle in the schematic. Error bars represent standard deviations of 3 technical replicates. (B) Two-hour TX-TL time course trajectories of constructs containing the wild type pT181 attenuator followed by an SFGFP coding sequence (WT-att), compared with a mutated version of the pT181 attenuator (Mut-att) followed by an SFGFP coding sequence. The effective model simulates these two constructs with identical ODEs. Therefore, the two trajectories are expected to overlay each other if the DNA qualities of these two constructs are comparable. The result confirmed that this modeling approach is valid. Error bars represent standard deviations of 9 technical replicates.

Supplementary Note 1: ODEs that model individual parameterization experiments.

To estimate all unknown parameters, we proposed 5 TX-TL experiments to be performed sequentially following[2] (See Figure4, Figure S4). Each experiment contained DNA that encoded parts of the attenuator circuitry that was described by a set of ODEs shown below. All parameters and ODE species are listed in Tables S2 and S3. Note that K_{C2} is not parameterized directly, It is estimated assuming $K_{C2}/K_{C1}=K_2/K_1$ following[2].

Experiment 1:

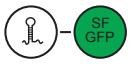

$$\frac{dM}{dt} = \beta_m \cdot (1 - P_t) - d_M \cdot M \tag{1.1}$$

$$\frac{dG}{dt} = k_t \cdot M - \alpha \cdot G \tag{1.2}$$

$$\frac{dG_M}{dt} = \alpha \cdot G \tag{1.3}$$

Experiment 2:

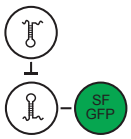

$$\frac{dR_1^*}{dt} = \beta_R - d_1 \cdot R_1^* - r_{m1} \cdot R_1^* \tag{2.1}$$

$$\frac{dR_1}{dt} = r_{m1} \cdot R_1^* - d_1 \cdot R_1 \tag{2.2}$$

$$\frac{dM}{dt} = \beta_m \cdot (1 - P_t) \cdot (1 - \frac{R_1}{K_1 + R_1}) - d_M \cdot M \tag{2.3}$$

$$\frac{dG}{dt} = k_t \cdot M - \alpha \cdot G \tag{2.4}$$

$$\frac{dG_M}{dt} = \alpha \cdot G \tag{2.5}$$

Experiment 3:

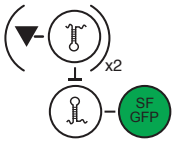

$$\frac{dR_2^*}{dt} = \beta_R - d_2 \cdot R_2^* - r_{m2} \cdot R_2^* \tag{3.1}$$

$$\frac{dR_2}{dt} = r_{m2} \cdot R_2^* - d_2 \cdot R_2 \tag{3.2}$$

$$\frac{dM}{dt} = \beta_m \cdot (1 - P_t) \cdot (1 - \frac{R_2}{K_2 + R_2}) - d_M \cdot M \tag{3.3}$$

$$\frac{dG}{dt} = k_t \cdot M - \alpha \cdot G \tag{3.4}$$

$$\frac{dG_M}{dt} = \alpha \cdot G \tag{3.5}$$

Experiment 4:

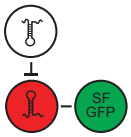

$$\frac{dR_1^*}{dt} = \beta_R - d_1 \cdot R_1^* - r_{m1} \cdot R_1^* \tag{4.1}$$

$$\frac{dR_1}{dt} = r_{m1} \cdot R_1^* - d_1 \cdot R_1 \tag{4.2}$$

$$\frac{dM}{dt} = \beta_m \cdot (1 - P_t) \cdot (1 - \frac{R_1}{K_{C1} + R_1}) - d_M \cdot M \tag{4.3}$$

$$\frac{dG}{dt} = k_t \cdot M - \alpha \cdot G \tag{4.4}$$

$$\frac{dG_M}{dt} = \alpha \cdot G \tag{4.5}$$

Experiment 5:

$$\frac{dMG^*}{dt} = \beta \cdot (1 - P_t) - d_{MG} \cdot MG^* - r_b \cdot MG^* \tag{5.1}$$

$$\frac{dMG}{dt} = r_b \cdot MG^* - d_{MG} \cdot MG \tag{5.2}$$

Supplementary Note 2: Methods for sensitivity analysis and parameter identifiability.

Below we outline our methods for identifying parameters that can be fit from specifically designed experiments following[2]. Our model for RNA circuitry consists of a set of ordinary differential equations that describe the time-dependent rates of concentration changes of the molecular species that participate in the circuitry, $x_i(t)$. These equations are parameterized by a set of parameters, p_j, that we want to estimate by fitting model predictions to a small set of experiments. These experiments were designed through an iterative process of sensitivity analysis on the set of model equations (Figure S4).

An individual experiment was considered to be a TX-TL reaction containing a subset of the DNA constructs encoding the full sRNA transcriptional NAR at defined concentrations. Each such experiment produces a measurable trajectory of SFGFP fluorescence as a function of time, and can be modeled by the subset of equations that describe the gene expression processes from the included DNA. After a specific experiment (a subset of DNA) was proposed, the next step was to assess which parameters were 'identifiable' from this experiment, which is closely linked with parametric sensitivity analysis. Here we used the procedure proposed by McAuley and coworkers[3] to first calculate and analyze the sensitivity coefficient matrix for the proposed experiment as follows.

For each experiment, the sensitivity coefficient matrix $z_{ij}(t)$, is a time-varying matrix that encapsulates how sensitive the concentration of the molecular species x_i is to a change in the parameter p_j

$$z_{ij}(t) = \left.\frac{\partial x_i}{\partial p_j}\right|_t \qquad i = 1,2,\ldots,N \quad j = 1,2,\ldots,P$$

Here P denotes the number of parameters and N denotes the number of molecular species. If we write the model equations generally as

$$\frac{dx_i}{dt} = f_i(\boldsymbol{x},\boldsymbol{p},t)$$

then it can be shown that $Z_{ij}(t)$ are the solutions to a set of differential equations given by

$$\frac{dz_{i,j}}{dt} = \sum_{k=1}^{N} \frac{\partial f_i}{\partial x_k}(\boldsymbol{x},\boldsymbol{p},t) z_{k,j} + \frac{\partial f_i}{\partial p_j}(\boldsymbol{x},\boldsymbol{p},t)$$

which are subject to the initial condition $z_{ij}(0) = 0$. Since our only observable in the TX-TL experiment is SFGFP, we focused specifically on $z_{SFGFP,j}(t)$ to determine which parameters were identifiable in the experiment.

Identifiability was then performed according to McAuley[3].This was done by finding the column of this matrix that had the biggest magnitude (indicating the most sensitive parameter), calculating a residual matrix which removed this column and controlled for correlations between parameters, and iterating this procedure on the resulting residual matrix until a threshold was reached on the largest remaining column magnitude. In this way a set of parameters was determined that maximally influenced the modeled trajectory of the proposed experiment (Figure 4).

After performing this procedure on the simplest experiment (experiment 1), we proposed a further experiment and performed the same analysis, except that parameters already identified by previous experiments were marked as 'determined' by setting their columns in the sensitivity

matrix to 0. Rounds of experimental design and sensitivity analysis were performed until all 16 parameters were able to be identified by five TX-TL experiments (Figure 4, Figure S4).

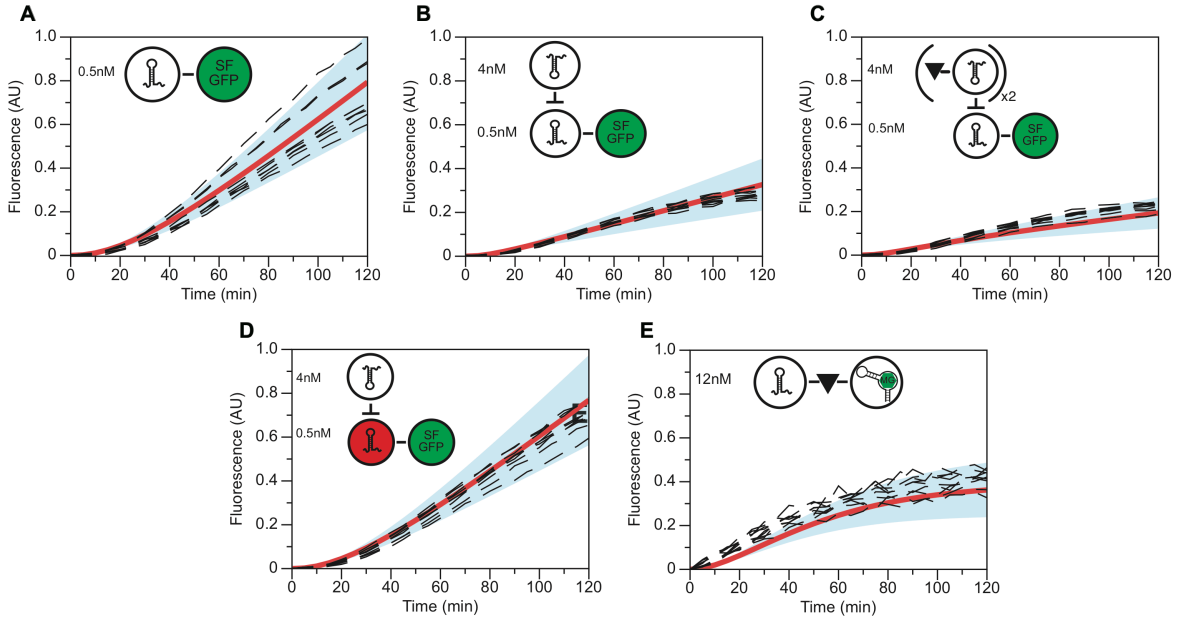

Figure S4. Validation of model simulations of parameter estimation experiments. Comparison of experimental trajectories of SFGFP (or MG) fluorescence in TX-TL experiments (black dashed lines) with simulated model predictions. Model simulated trajectories were generated by performing 1000 simulations with parameters drawn from the set of 10,000 determined from the estimation procedure (see Methods). Experimental and model trajectories were normalized by the maximum observed experimental fluorescence of the first experiment in (A). The mean simulated trajectory (red line) is shown within 95% confidence intervals derived from the range of simulated trajectories (blue region). The schematic of each experiment is shown in the upper left corner of each plot corresponding to the experiments in Figure 4 and equations in Supplementary Note 1.

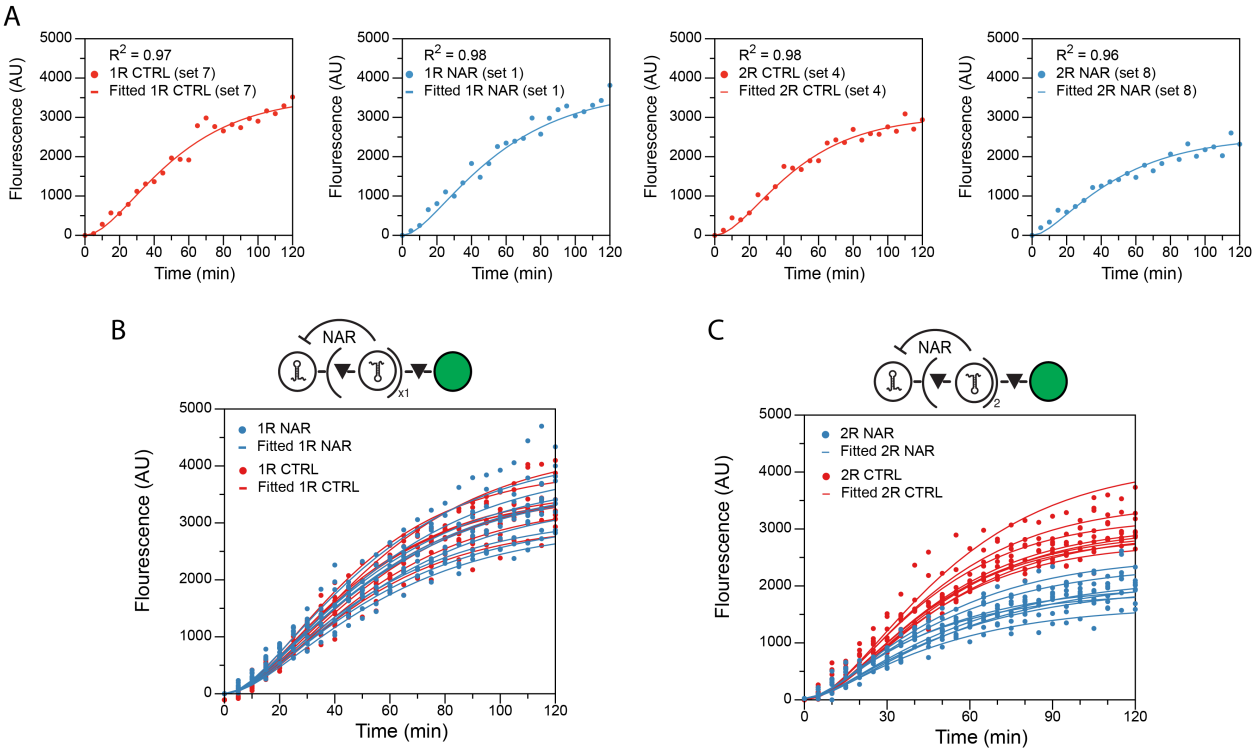

Figure S5. Response time estimation procedure. To estimate the response time of dynamic trajectories generated by constructs in TX-TL reactions, we used a least squares method to approximate when each trajectory reaches steady state (see Methods). Since the raw data contains experimental noise within individual trajectories, steady state approximation is a difficult task. To overcome this, we fitted the data with our model and used the best fit trajectory to estimate the response time. (A) We searched for the best trajectory for each individual experimental replicate based on best R^2 values. Sample fitting trajectories and experimental data from each experiment are shown. (B) All fitted trajectories and experimental data from the single repressor NAR vs. control constructs. (C) All fitted trajectories and experimental data from the double repressor NAR vs. control constructs. Response time of each experimental replicate (shown in Figure 5) was calculated independently following the least squared method (See Methods).

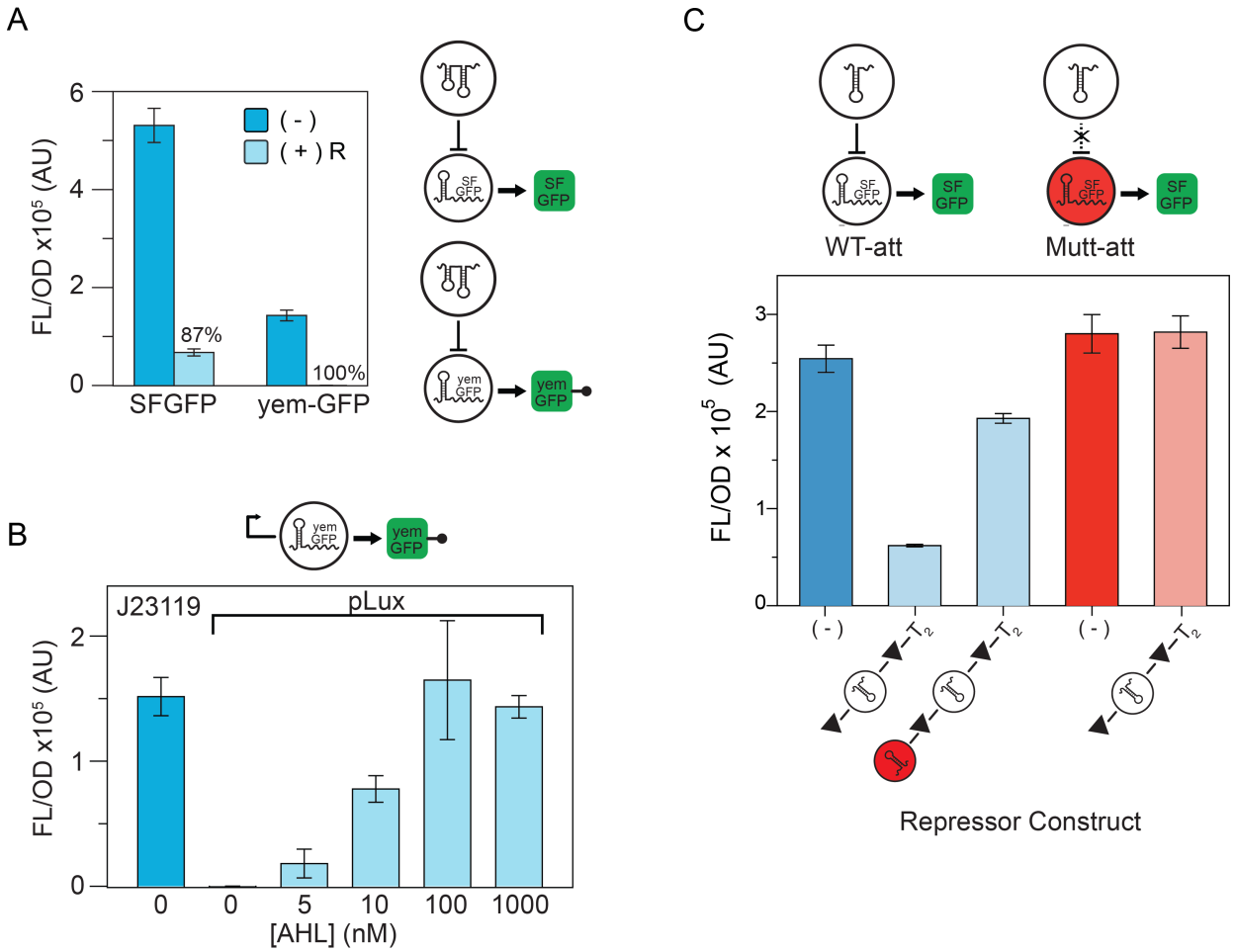

Figure S6. Parts tested for the sRNA transcriptional NAR networks designed for *in vivo* experiments. (A) Testing yem-GFP in the context of the sRNA repressor. Expression was characterized from constructs containing a constitutive promoter followed by a pT181 attenuator and either GFP or yem-GFP with a control plasmid (-), or a plasmid encoding a cognate sRNA repressor (R,+). Results showed an improvement in repression strength when yem-GFP was used. Error bars represent standard deviations over nine biological replicates. (B) Using AHL to titrate expression of an attenuator construct. The attenuator-yem-GFP construct was placed behind the AHL inducible promoter pLux. Construct expression was measured after induction with a range of AHL concentrations after 5 hours, and compared to a constitutively expressed construct (J23119). The results confirmed a range of AHL induction levels of this repressor expression construct. Later *in vivo* experiments were performed with 100nM of AHL based on this result. Error bars represent standard deviations over nine biological replicates. (C) Repression efficiency of the single repressor construct used in the single repressor NAR networks. The repression strength of a single repressor flanked by ribozymes (triangle) versus the same construct with a mutant attenuator placed upstream. The present of the mutant attenuator significantly reduces the repression strength. Testing the repressor construct against a mutant attenuator target region (red bars) showed that the repression inefficiency was not due to crosstalk, but is rather due to the attenuator causing reduced sRNA transcription (see Figure S2A). Error bars represent standard deviations over three technical replicates.

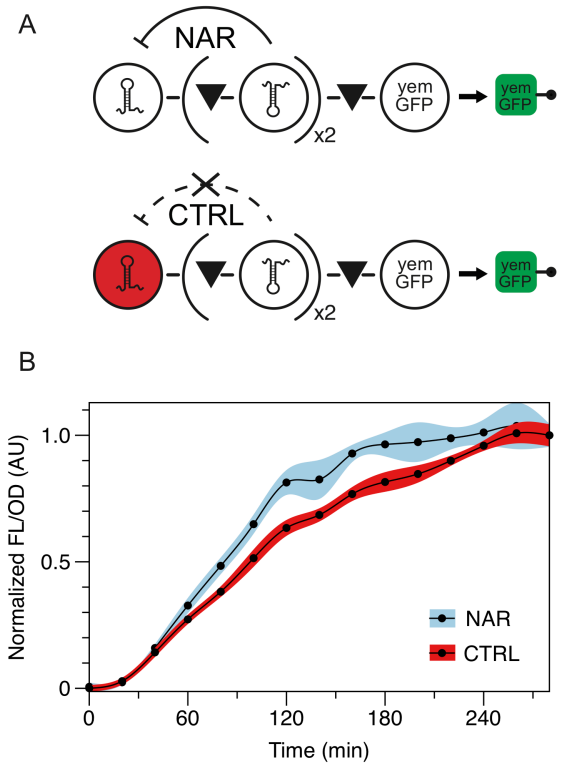

Figure S7. Characterization of double repressor sRNA transcriptional NAR networks *in vivo* with normalized data. (A) Schematics of the double repressor NAR and control constructs designed for *in vivo* testing using yem-GFP as a network reporter. (B) Normalized trajectories collected from *E. coli* TG1 cells containing the double repressor NAR (blue) or control (red) construct over a five-hour period. Each experimental replicate from Figure 6B was normalized to its steady state value to show that NAR speeds up network response time.

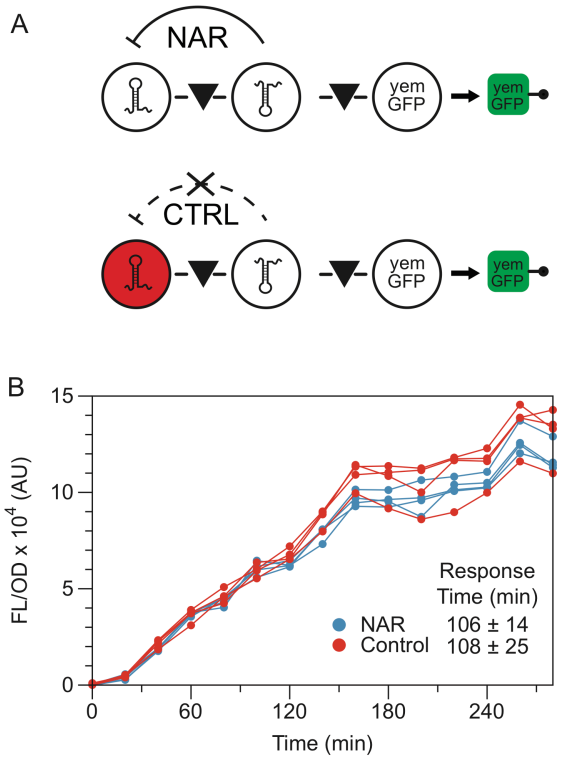

Figure S8. Characterization of single repressor sRNA transcriptional NAR *in vivo*. (A) Schematics of the single repressor NAR and control constructs designed for *in vivo* testing using yem-GFP as a network reporter. (B) Four replicate fluorescence (FL/OD) trajectories collected from *E. coli* TG1 cells containing the single repressor NAR (blue) or control (red) construct over a five-hour period. In this case, no clear speed up in response was observed.

Table S1 Parameters guesses from previous work [2]

Parameter	Single-R	Tandem-R	Definition	Unit
1. β	1.5	1.5	Rate of transcription	AU Conc./sec
2. K	600	300	Repression co-efficient of RNA repressor	AU Conc.
3. d	0.008	0.004	Repressor degradation rate	1/sec
4. dm	0.006	0.006	Reporter (G) degradation rate	1/sec

Table S2 All parameters involved in parameterization procedure

#	Parameter**	Description	Estimated Value	Unit
P(1)	β_m	Transcription rate of mRNA	4.9 ± 0.41	Conc./sec.
P(2)	K_1	Repression coefficient of single repressor	289.5 ± 24.9	Conc.
P(3)	K_2	Repression coefficient of double (tandem) repressor	193.6 ± 16.7	Conc.
P(4)	K_{C1}	Repression coefficient of mismatched repressor due to crosstalk	10113.5 ± 886.0	Conc.
P(5)	d_1	Degradation rate of single repressor	2.1e-03 ± 2.8e-04	1/sec.
P(6)	r_{m1}	Maturation rate of single repressor	6.9e-05 ± 5.9e-06	1/sec.
P(7)	r_{m2}	Maturation rate of double repressor	7.5e-05 ± 6.4e-06	1/sec.
P(8)	r_b	Maturation and binding rate of MG	1.3e-04 ± 1.1-e05	1/sec.
P(9)	β_R	Transcription rate of repressor	39.4 ± 3.3	Conc./sec.
P(10)	k_t	Translational rate of SFGFP	2.6e-04 ± 2.3e-05	1/sec.
P(11)	α	Maturation rate of SFGFP	1.7e-02 ± 1.4e-03	1/sec.
P(12)	d_M	Degradation Rate of SFGFP mRNA	5.9e-04 ± 5.1e-05	1/sec.
P(13)	β	Transcription rate of pre-cleaved MG	16.0 ± 1.4	Conc./sec.
P(14)	d_{MG}	Degradation rate of MG RNA	5.3e-04 ± 4.6e-05	1/sec.
P(15)	d_2	Degradation rate of double repressor	1.7e-03 ± 1.4e-04	1/sec.
P(16)	P_t	Auto-termination probability*	0.18 ± 0.016	N/A

* In our previous work, we observed inefficient transcription when an antisense sRNA was placed downstream of an attenuator[1,2,4]. It was described as "auto-termination", but the detailed mechanism behind this observation is not fully understood, which could also be caused by random RNA polymerase fall off due to the transcription of extra sequence. Correspondingly in this work, we also observed the same inefficiency of transcription when a RNA is placed downstream of a repressor RNA sequence (Figure S3A). We therefore used the same parameter when modeling this feature of our networks in each scenario. In particular, the P_t parameter (inefficiency in transcription caused by attenuator) was estimated to be 18% ± 1.6% and the inefficiency in transcription caused by repressor sRNA was found to be approximately 19.1% from a TX-TL experiment designed to measure this effect (Figure S3A). Since the two parameters are very similar, we lumped them together as one parameter for simplicity.
**NAR involved parameters are highlighted in red.

Table S3: Model Species

Model Species	Definition
R_1^*	Immature single sRNA repressor
R_1	Mature single sRNA repressor
R_2^*	Immature double (tandem) sRNA repressor
R_2	Mature double (tandem) repressor
M	mRNA of SFGFP
G	Immature SFGFP
G_M	Mature SFGFP
MG*	Pre-cleaved R- MG
MG	Cleaved-off MG

Table S4 Important DNA sequences.

Name	Sequence
ECK125109870 terminator	ccaattattgAACACCCTAACGGGTGTTTTTTTGTTTctggtctccc
L3S1P22 terminator	GACGAACAATAAGGCCGCAAATCGCGGCCTTTTTTATTGATAACAAAA
L3S3P21 terminator	CCAATTATTGAAGGCCTCCCTAACGGGGGGCCTTTTTTTGTTTCTGGTCTCCC
L3S3P47 terminator	TTTTCGAAAAAACACCCTAACGGGTGTTTTTTTATAGCTGGTCTCCC
Yem-GFP-LAA protein with degradation tag LAA	atgtctaaaggtgaagaattattcactggtgttgtcccaattttggttgaattagatggtgatgttaatggtcacaaattttctgtctccggtgaaggtgaaggtgatgctacttacggtaaattgaccttaaaatttatttgtactactggtaaattgccagttccatggccaaccttagtcactactttaacttatggtgttcaatgtttttctagatacccagatcatatgaaacaacatgacttttcaagtctgccatgccagaaggttatgttcaagaaagaactatttttttcaaagatgacggtaactacaagaccagagctgaagtcaagtttgaaggtgataccttagttaatagaatcgaattaaaaggtattgattttaaagaagatggtaacattttaggtcacaaattggaatacaactataactctcacaatgtttacatcatggctgacaaacaaaagaatggtatcaaagttaacttcaaaattagacacaacattgaagatggttctgttcaattagctgaccattatcaacaaaatactccaatttggtgatggtccagtcttgttaccagacaaccattacttatccactcaatctaaattatccaaagatccaaacgaaaagagagaccacatggtcttgttagaatttgttactgctgctggtattaccccatggtatggatgaattgtacaaaACTAGTGCAGCGAACGACGAAAATTACGCCCTTGCAGCG
T1 terminator	gcatcaaataaaacgaaaggctcagtcgaaagactgggcctttcgttttatctgttgtttgtcggtgaacgctctcctgagtaggacaaatccgccgccctagac
pLux promoter	acctgtaggatcgtacaggtttacgcaagaaaatggtttgttatagtcgaataaa
LuxR	atgaaaaacataaatgccgacgacacatacagaataattaataaaattaaagcttgtagaagcaataatgatattaatcaatgcttatctgatatgactaaaatggtacattgtgaatattattactcgcgatcatttatcctcattctatggttaaatctgatatttcaatcctagataattacccctaaaaaatggaggcaatattatgatgacgctaatttaataaaatatgatcctatagtagattattctaactccaatcattcaccaattaattggaatatatttgaaaacaatgctgtaaataaaaaatctccaaatgtaattaaagaagcgaaaacatcaggtcttatcactgggtttagtttccctattcatacggctaacaatggcttcggaatgcttagttttgcacattcagaaaaagacaactatatagatagtttatttttacatgcgtgtatgaacataccattaattgttccttctctagttgataattatcgaaaaataaatatagcaaataataaatcaaacaacgatttaaccaaaagagaaaaagaatgtttagcgtgggcatgcgaaggaaaaagctcttgggatatttcaaaaatattaggttgcagtgagcgtactgtcactttccatttaaccaatgcgcaaatgaaactcaatacaacaaaccgctgccaaagtatttctaaagcaattttaacaggagcaattgattgcccatactttaaaaattaa
Malachite green aptamer (MG)	GGGATCCCGACTGGCGAGAGCCAGGTAACGAATGGATC

pT181 R(H2) single hairpin repressor	tctttgaatgatgtcgttcacaaactttggtcagggcgtgagcgactccttttattt
Mut pT181 R(H2), mutant single hairpin repressor	tctttgaatgatgtcgttcTGCaactttggCGagggACAgagcgactccttttattt
pT181-attenuator	AACAAAATAAAAAGGAGTCGCTCACGCCCTGACCAAAGTTT GTGAACGACATCATTCAAAGAAAAAAACACTGAGTTGTTTTT ATAATCTTGTATATTTAGATATTAAACGATATTTAAATATACAT AAAGATATATATTTGGGTGAGCGATTCCTTAAACGAAATTGA GATTAAGGAGTCGCTCTTTTTTATGTATAAAAACAATCATGCA AATCATTCAAATCATTTGGAAAATCACGATTTAGACAATTTTT CTAAAACCGGCTACTCTAATAGCCGGTTGTAA
pT181-mutant attenuator	AACAAAATAAAAAGGAGTCGCTCTGTCCCTCGCCAAAGTTG CAGAACGACATCATTCAAAGAAAAAAACACTGAGTTGTTTTT ATAATCTTGTATATTTAGATATTAAACGATATTTAAATATACAT AAAGATATATATTTGGGTGAGCGATTCCTTAAACGAAATTGA GATTAAGGAGTCGCTCTTTTTTATGTATAAAAACAATCATGCA AATCATTCAAATCATTTGGAAAATCACGATTTAGACAATTTTT CTAAAACCGGCTACTCTAATAGCCGGTTGTAA
Super folder green fluorescent protein (Ribosome binding site - SFGFP)	AGGAGGAAGGATCTATGAGCAAAGGAGAAGAACTTTTCACT GGAGTTGTCCCAATTCTTGTTGAATTAGATGGTGATGTTAAT GGGCACAAATTTTCTGTCCGTGGAGAGGGTGAAGGTGATGC TACAAACGGAAAACTCACCCTTAAATTTATTTGCACTACTGG AAAACTACCTGTTCCGTGGCCAACACTTGTCACTACTCTGAC CTATGGTGTTCAATGCTTTTCCCGTTATCCGGATCACATGAA ACGGCATGACTTTTTCAAGAGTGCCATGCCCGAAGGTTATG TACAGGAACGCACTATATCTTTCAAAGATGACGGGACCTACA AGACGCGTGCTGAAGTCAAGTTTGAAGGTGATACCCTTGTT AATCGTATCGAGTTAAAGGGTATTGATTTTAAAGAAGATGGA AACATTCTTGGACACAAACTCGAGTACAACTTTAACTCACAC AATGTATACATCACGGCAGACAAACAAAAGAATGGAATCAAA GCTAACTTCAAAATTCGCCACAACGTTGAAGATGGTTCCGTT CAACTAGCAGACCATTATCAACAAAATACTCCAATTGGCGAT GGCCCTGTCCTTTTACCAGACAACCATTACCTGTCGACACAA TCTGTCCTTTCGAAAGATCCCAACGAAAAGCGTGACCACAT GGTCCTTCTTGAGTTTGTAACTGCTGCTGGGATTACACATGG CATGGATGAGCTCTACAAATAA
TrrnB	GAAGCTTGGGCCCGAACAAAAACTCATCTCAGAAGAGGATC TGAATAGCGCCGTCGACCATCATCATCATCATCATTGAGTTT AAACGGTCTCCAGCTTGGCTGTTTTGGCGGATGAGAGAAGA TTTTCAGCCTGATACAGATTAAATCAGAACGCAGAAGCGGTC TGATAAAACAGAATTTGCCTGGCGGCAGTAGCGCGGTGGTC CCACCTGACCCCATGCCGAACTCAGAAGTGAAACGCCGTAG CGCCGATGGTAGTGTGGGGTCTCCCCATGCGAGAGTAGGG AACTGCCAGGCATCAAATAAAACGAAAGGCTCAGTCGAAAG ACTGGGCCTTTCGTTTTATCTGTTGTTTGTCGGTGAACT
pT181 WT repressor	ATACAAGATTATAAAAACAACTCAGTGTTTTTTTCTTTGAATG ATGTCGTTCACAAACTTTGGTCAGGGCGTGAGCGACTCCTT TTTATTT

sTRSV Ribozyme	CTGTCACCGGATGTGCTTTCCGGTCTGATGAGTCCGTGAGGACGAAACAG
J23119 constitutive promoter	TTGACAGCTAGCTCAGTCCTAGGTATAATACTAGT

Table S5 Plasmids used in this study. Sequences in the plasmid architecture can be found in Table S4.

Plasmid #	Plasmid architecture	Name	Figure
JBL3329	J23119-Att-yemGFP-LAA-T1 CmR/p15A	Yem-GFP	S6A
JBL3349	pLuxR - pT181 Att - yem-GFP-LAA-T1 CmR/p15A	pLux-Yem-GFP	S6B
JBL3396	pLux - pT181 Att - sTRSV - pT181 R(H2)* - sTRSV - pT181 R(H2) - sTRSV - yemGFP-LAA	Double Repression NAR network in vivo	6, S7
JBL3398	pLuxR - pT181 Att mut - sTRSV - pT181 R(H2) - sTRSV - pT181 R(H2) - sTRSV - yemGFP-LAA	Double Repression NAR CTRL network in vivo	6, S7
JBL3368	pLux - pT181 Att - sTRSV - pT181 R(H2) - sTRSV - yemGFP-LAA	Single Repression NAR network in vivo	S8
JBL3399	pLuxR - pT181 Att mut - sTRSV - pT181 R(H2) - sTRSV - yemGFP-LAA	Single Repression NAR CTRL network in vivo	S8
JBL3343	J23119 -sTRSV rbz-pT181 R(H2)-sTRSV rbz-L3S3P21Term	Truncated pT181 repressor, parameterization experiment 2	4,2B,2A,S6C
JBL5020	J23119 - sTRSV - pT181 R(H2) - sTRSV - pT181 R(H2) - sTRSV - L3S3P21T	2Xtruncated pT181 repressor, parameterization experiment 3	4, S1D
JBL3339	J23119 -sTRSV rbz-pT181 R(H2)-L3S3P21Term	Truncated pT181 repressor, no ribozyme before terminator	2B,2A
JB:5024	sTRSV-mut pT181 R(H2) - sTRSV-P21T	Truncated pT181 mutated repressor	2B
JBL5025	sTRSV-mut pT181 R(H2)-P21T	Truncated pT181 mutated repressor,no ribozyme before terminator	2B
JBL006	J23119 – pT181 att – SFGFP – TrrnB – CmR – p15A origin	pT181 attenuator, Att-1 Parameterization experiment 1	4,S1D,S3B,S6C
JBL002	J23119 – TrrnB – ColE1 origin – AmpR	No repressor control	4, S6C
JBL007	J23119 – pT181 att mut – SFGFP – TrrnB – CmR – p15A origin	pT181 mutant attenuator, parameterization experiment 4	4, S3B, S6C
JBL004	J23119 – pT181 R – TrrnB – ColE1 origin – AmpR	pT181 repressor	2A
JBL1885	J23119-pT181-R ECK125109870 term - – ColE1 origin – AmpR	Terminator variant	S1C

JBL1886	J23119-pT181-R L3S1P22 term - – ColE1 origin – AmpR	Terminator variant	S1C
JBL1887	J23119-pT181-R L3S3P21 term- – ColE1 origin – AmpR	Terminator variant	S1C,2A
JBL1888	J23119-pT181-R L3S3P47 term- – ColE1 origin – AmpR	Terminator variant	S1C
JBL3375	J23119 - pT181 Att - sTRSV - pT181 R(H2) - sTRSV - MG - L3S3P21T	Single Repression NAR network TX-TL	5,S7
JBL3376	J23119 - pT181 Att - sTRSV - pT181 R(H2)- sTRSV - pT181 R(H2) - sTRSV - MG - L3S3P21T	Double Repression NAR network TX-TL	5,S7
JBL3377	J23119 - pT181 Att mut - sTRSV - pT181 R(H2) - sTRSV - MG - L3S3P21T	Single Repression NAR CTRL network TX-TL	5,S7
JBL3378	J23119 - pT181 Att mut - sTRSV - pT181 R(H2) - sTRSV - pT181 R(H2) - sTRSV - MG - L3S3P21T	Double Repression NAR CTRL network TX-TL	5,S7
JBL3358	J23119 - pT181 R(H2) - sTRSV - MG - L3S3P21T	R-MG	S3A
JBL5032	J23119 - MG - L3S3P21T	MG	S3A
JBL3326	pT181- pT181 R(H2)- L3S3P21 term	Truncated pT181 repressor	2A
JBL3355	J23119 - sTRSV - pT181 R(H2) - sTRSV - pT181 R(H2) - L3S3P21T	2X truncated pT181 repressor, no ribozyme before terminator	2A, S1D
JBL5054	J23119 - pT181 Att mutH1 - sTRSV - RWT(H2) - sTRSV- L3S3P21T	Mutated attenuator followed by 1 truncated pT181 repressor, with ribozyme before terminator	S6C

References

(1) Lucks, J. B., Qi, L., Mutalik, V. K., Wang, D., Wang, D., and Arkin, A. P. (2011) Versatile RNA-sensing transcriptional regulators for engineering genetic networks. *Proc. Natl. Acad. Sci. U.S.A. 108*, 8617–8622.

(2) Hu, C. Y., Varner, J. D., and Lucks, J. B. (2015) Generating Effective Models and Parameters for RNA Genetic Circuits. *ACS Synth Biol 4*, 914–926.

(3) Yao, K. Z., Shaw, B. M., Kou, B., McAuley, K. B., and Bacon, D. W. (2003) Modeling Ethylene/Butene Copolymerization with Multi-site Catalysts: Parameter Estimability and Experimental Design. *Polymer Reaction Engineering 11*, 563–588.

(4) Takahashi, M. K., Chappell, J., Hayes, C. A., Sun, Z. Z., Kim, J., Kim, J., Singhal, V., Singhal, V., Spring, K. J., Spring, K. J., Al-Khabouri, S., Al-Khabouri, S., Fall, C. P., Fall, C. P., Noireaux, V., Murray, R. M., and Lucks, J. B. (2015) Rapidly Characterizing the Fast Dynamics of RNA Genetic Circuitry with Cell-Free Transcription-Translation (TX-TL) Systems. *ACS Synth Biol 4*, 503–515.